

Model investigations of the correlation between the mean transverse momentum and anisotropic flow in shape-engineered events

Niseem Magdy¹ and Roy A. Lacey²

¹*Department of Physics, University of Illinois at Chicago, Chicago, Illinois 60607, USA*

²*Department of Chemistry, State University of New York, Stony Brook, New York 11794, USA*

Abstract

The correlation between the event mean-transverse momentum [p_T], and the anisotropic flow magnitude v_n , $\rho(v_n^2, [p_T])$, has been argued to be sensitive to the initial conditions in heavy-ion collisions. We use simulated events generated with the AMPT and EPOS models for Au+Au at $\sqrt{s_{NN}} = 200$ GeV, to investigate the model dependence and the response and sensitivity of the $\rho(v_2^2, [p_T])$ correlator to collision-system size and shape, and the viscosity of the matter produced in the collisions. We find good qualitative agreement between the correlators for the string melting version of the AMPT model and the EPOS model. The model investigations for shape-engineered events as well as events with different viscosity (η/s), indicate that $\rho(v_2^2, [p_T])$ is sensitive to the initial-state geometry of the collision system but is insensitive to sizable changes in η/s for the medium produced in the collisions. These findings suggest that precise differential measurements of $\rho(v_2^2, [p_T])$ as a function of system size, shape, and beam-energy could provide more stringent constraints to discern between initial-state models and hence, more reliable extractions of η/s .

A central objective of the current heavy-ion programs at the Large Hadron Collider (LHC) and the Relativistic Heavy-Ion Collider (RHIC) is to understand the transport properties of the quark-gluon plasma (QGP) [1, 2, 3] formed in high-energy heavy-ion collisions. In recent years, particular attention has been given to precision extraction of the specific shear viscosity of the QGP - the ratio of shear viscosity η , to the entropy density s , (η/s). The specific shear viscosity encodes the ability of the QGP to transport momentum. In general observables that characterize the azimuthal anisotropy of particles emitted in the transverse plane, are among the key measurements that have been used to constrain the viscous hydrodynamic response to the initial spatial distribution in energy density, produced in the early stages of the collision [4, 5, 6, 7, 8, 9, 10, 11, 12, 13, 14, 15, 16, 17, 18, 19, 20, 21].

These studies indicated that a significant uncertainty in the η/s extractions stems from the uncertainty in the estimates for the initial-state eccen-

tricities employed in the model calculations. Subsequently, several works have sought to construct and investigate new observables insensitive to η/s and more sensitive to initial-state effects leading to new constraints for the initial-state models [22, 23].

One such observable, that leverages the correlation between the n^{th} -order flow harmonics v_n , and the average transverse momentum of particles in an event [p_T], is the correlation coefficient $\rho(v_n^2, [p_T])$ [22, 24, 25, 26, 27, 28, 29];

$$\rho(v_n^2, [p_T]) = \frac{\text{cov}(v_n^2, [p_T])}{\sqrt{\text{Var}(v_n^2)} \sqrt{\text{Var}([p_T])}}. \quad (1)$$

Here, v_n is eccentricity-driven and the [p_T] is related to the transverse size of the overlap region, so events that have similar energy-density but smaller initial-state transverse size should have a larger radial expansion and consequently larger mean transverse momentum [30]. It has also been proposed that the $\rho(v_n^2, [p_T])$ correlator is sensitive to the correlations between the initial size and the initial-state deformation of colliding nuclei [29, 31, 32].

Initial measurements of the $\rho(v_n^2, [p_T])$ correlator have been reported for p+Pb and Pb+Pb collisions

¹niseemm@gmail.com

at $\sqrt{s_{NN}} = 5.02$ TeV by the ATLAS Collaboration [33]. In Pb+Pb collisions the leading order experimental trend for $\rho(v_2^2, [p_T])$ reflected negative values in peripheral or very low multiplicity events, but increased with centrality to positive values for mid to central collisions. These measurements provided important insights for initial-state models at LHC energies. The $\rho(v_2^2, [p_T])$ correlator has also been studied in hydrodynamic and transport models [25, 27, 28, 34]. Nonetheless, further detailed studies of $\rho(v_n^2, [p_T])$ are required to optimize its utility to discern between different initial-state models.

In this work, we use detailed simulations with both the AMPT [35], and EPOS [36, 37, 38] models for Au+Au at $\sqrt{s_{NN}} = 200$ GeV, to study the $\rho(v_2^2, [p_T])$ correlators model dependence and its response and sensitivity to the magnitude of η/s and initial-state geometry. We exploit the technique of event-shape engineering to obtain a more detailed influence of the initial-state geometry. Our study emphasizes investigations for Au+Au collisions at $\sqrt{s_{NN}} = 200$ GeV in anticipation of the need for model predictions to compare to upcoming experimental measurements.

This study is performed with simulated events for Au+Au collisions at $\sqrt{s_{NN}} = 200$ GeV, obtained with the AMPT [35], and EPOS [36, 37, 38] models. Computations were performed for charged hadrons in the transverse momentum range $0.2 < p_T < 2.0$ GeV/c and the pseudorapidity acceptance $|\eta| < 1.0$. The latter choice mimics the acceptance of the STAR experiment at RHIC.

- **AMPT Model:** The AMPT model(version 2.26t9b) [35] has been widely used to study relativistic heavy-ion collisions at LHC and RHIC energies [35, 39, 40, 41, 42, 43, 44, 45, 46, 47]. In the current study, simulations were made with the string melting option both on and off. In such a situation when the string melting mechanism is on, hadrons created from the HIJING model are converted to their valence quarks and anti-quarks, and their evolution in time and space is then shaped by the ZPC parton cascade model [48]. The key elements of AMPT include (i) HIJING model [49, 50] initial parton-production stage , (ii) a parton scattering stage, (iii) hadronization through coalescence followed by (iv) a hadronic interaction stage [51]. In stage (ii) the used parton scattering cross-sections are evaluated accord-

ing to;

$$\sigma_{pp} = \frac{9\pi\alpha_s^2}{2\mu^2}, \quad (2)$$

where α_s is the QCD coupling constant and μ is the screening mass in the partonic matter. They principally establish the expansion dynamics of the A+A collision systems [48]; Within the AMPT model framework, the η/s value can be adjusted via an appropriate choice of μ and/or α_s for a particular initial temperature T_i [52].

$$\frac{\eta}{s} = \frac{3\pi}{40\alpha_s^2} \frac{1}{\left(9 + \frac{\mu^2}{T^2}\right) \ln\left(\frac{18 + \mu^2/T^2}{\mu^2/T^2}\right) - 18}, \quad (3)$$

In the current work, Au+Au collisions at $\sqrt{s_{NN}} = 200$ GeV, were simulated with model version ampt-v2.26t9b for a fixed value $\alpha_s = 0.47$, but the shear viscosity η/s is varied over the range 0.1–0.3 by adjusting μ from $2.26 - 4.2 \text{ fm}^{-1}$ for a temperature $T_i = 378 \text{ MeV}$ [52]. The three AMPT sets which will be presented in this work are summarized in Tab. 1.

AMPT-set	η/s	String Melting Mechanism
Set-1	0.1	OFF
Set-2	0.1	ON
Set-3	0.3	ON

Table 1: The summary of the three AMPT sets which will be presented in this work.

- **EPOS Model:** The EPOS model [36, 37, 38] is based on a 3+1D viscous hydrodynamical description of A+A collisions. The initial state conditions are defined in terms of flux tubes estimated via Gribov-Regge multiple scattering theory [36]. EPOS can be subdivided into three main components, (i) the core-corona division, (ii) the hydrodynamical evolution, and (iii) the hadronic cascades.
 - (i) The separation of the flux tubes fragmentation into *core* and *corona* (hadronize as a hadron jet) is based on the probability to escape from the bulk matter which will depends on the fragment transverse momentum and the local string density.

(ii) The hydrodynamical evolution based on the *vHLLE*, viscous HLLE-based algorithm, 3D+1viscous hydrodynamics employ a realistic Equation of State constrained with Lattice QCD data [53].

(iii) The hadronic cascade, *hadronic afterburner*, is based on the UrQMD model [54, 55], which has been broadly employed to investigate ultra-relativistic heavy-ion collisions [54, 55, 56]. UrQMD was designed to investigate hadron-hadron, hadron-nucleus, and heavy-ion collisions from $E_{\text{Lab}} = 100 \text{ A}\cdot\text{MeV}$ to $\sqrt{s_{\text{NN}}} = 200 \text{ GeV}$. Therefore, it includes a collision term that accounts for the interactions of more than 50 (40) baryon (meson) species as well as their anti-particles. The URQMD model describes the hadron-hadron interactions as well as the system evolution based on covariant propagation of all hadrons in the model with resonance decay, stochastic binary scattering, and color string formation.

The results reported in this work, were obtained for minimum bias Au+Au collisions at $\sqrt{s_{\text{NN}}} = 200 \text{ GeV}$. A total of approximately 4.0, 5.0, 3.0, and 0.3 M events of Au+Au collisions were generated with AMPT Set-1, Set-2, Set-3, and EPOS, respectively.

The $\rho(v_n^2, [p_T])$ correlator is derived from covariances and variances (cf. Eq. 1) which involve both two- and multi-particle correlations that could also be influenced by non-flow effects due to resonance decays, Bose-Einstein correlations, and the fragments of individual jets [57]. Since non-flow contributions mostly involve particles emitted within a localized region in pseudorapidity, η , they can be mitigated via the sub-event cumulant methods [44, 58, 59, 60]. A major mitigating feature of these methods, is the correlation of particles from two or more sub-events which are separated in η . The efficacy of these methods to reduce non-flow effects have been quantified for many different two- and multi-particle correlators [44, 58, 59]. It is noteworthy that these methods were used in the initial $\rho(v_n^n, [p_T])$ measurements by the ATLAS Collaboration [33].

In the current work, the two-subevents method is used to construct the v_2^2 variance. Thus, we use two separate η selections specified as $-1.0 < \eta_A < -0.35$ and $0.35 < \eta_C < 1.0$ to determine the v_2^2

variance as:

$$\begin{aligned} \text{Var}(v_2^2) &= v_2\{2\}^4 - v_2\{4\}^4, \\ &= C_2^2\{2\} - C_2\{4\}, \end{aligned} \quad (4)$$

where $v_2\{2\}$ and $v_2\{4\}$ are the flow coefficients obtained from the two- and four-particle correlations respectively, with the sub-event method [58] with particles in the region η_A and η_C ;

$$C_2\{2\} = \langle\langle 2 \rangle\rangle|_{A,C} = \langle\langle e^{i 2(\varphi_1^A - \varphi_2^C)} \rangle\rangle, \quad (5)$$

$$v_2\{2\} = \sqrt{C_n\{2\}} \quad (6)$$

where $\phi_{A(C)}$ is the azimuthal angle of particles in the region A (C).

$$C_2\{4\} = \langle\langle 4 \rangle\rangle|_{A,C} - 2\langle\langle 2 \rangle\rangle^2|_{A,C}, \quad (7)$$

$$v_2\{4\} = \sqrt[4]{-C_2\{4\}} \quad (8)$$

where,

$$\langle\langle 4 \rangle\rangle|_{A,C} = \langle\langle e^{i 2(\varphi_1^A + \varphi_2^A - \varphi_3^C - \varphi_4^C)} \rangle\rangle. \quad (9)$$

The variance of the dynamical p_T fluctuations [61], $c_k \sim \text{Var}([p_T])$, defined in region $|\eta_B| < 0.35$, can be given as:

$$c_k = \left\langle \frac{1}{N_{\text{pair}}} \sum_B \sum_{B' \neq B} (p_{T,B} - \langle [p_T] \rangle)(p_{T,B'} - \langle [p_T] \rangle) \right\rangle, \quad (10)$$

where $\langle \rangle$ is an average over all events. The event mean p_T , $[p_T]$, is given as,

$$[p_T] = \sum_{i=1}^{M_B} p_{T,i}/M_B, \quad (11)$$

where M_B is the event multiplicity in sub-event B . The covariance between v_2^2 and $[p_T]$, $\text{cov}(v_2^2, [p_T])$, is defined using the three-subevents method [33, 62] as,

$$\text{cov}(v_2^2, [p_T]) = \text{Re} \left(\left\langle \left\langle \sum_{A,C} e^{i 2(\phi_A - \phi_C)} ([p_T] - \langle [p_T] \rangle)_B \right\rangle \right\rangle \right). \quad (12)$$

The resulting $\rho(v_2^2, [p_T])$ correlator, obtained via Eqs. 4, 10 and 12;

$$\rho(v_2^2, [p_T]) = \frac{\text{cov}(v_2^2, [p_T])}{\sqrt{\text{Var}(v_2^2)} \sqrt{c_k}}, \quad (13)$$

is similar to that used in prior studies [22, 24, 25, 26, 27, 28, 29].

The $\rho(v_n^2, [p_T])$ correlator is derived from the correlations and fluctuations of v_n and p_T . Therefore, it is instructive to investigate the dependence of these variables on the models and the corresponding parameters

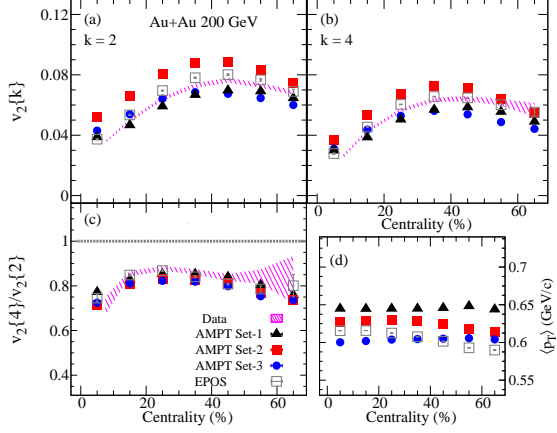


Figure 1: Centrality dependence of $v_2\{2\}$ (a), $v_2\{4\}$ (b), $v_2\{4\}/v_2\{2\}$ (c) and $\langle p_T \rangle$ computed with the AMPT and EPOS models for Au+Au collisions at 200 GeV. The hatched bands represent the experimental data reported by the STAR collaboration in Ref [63].

tabulated in Table 1. Fig. 1 shows a comparison of the centrality dependence of $v_2\{2\}$ (a), $v_2\{4\}$ (b) the ratios $v_2\{4\}/v_2\{2\}$ (c), and $\langle p_T \rangle$ (d) for the AMPT and EPOS models. Panels (a) and (b) indicate that the AMPT results are sensitive to both the viscosity and whether or not string melting is turned on. They also indicate similar qualitative patterns between both models and the data reported by the STAR collaboration [63] (hatched bands) over the range of the model parameters summarized in Table 1. Note that the experimental results are only shown for published data. An extraction of the $\langle p_T \rangle$ from the experimental charged hadrons spectra reported in Ref [64], indicates values which are closer to those obtained with the EPOS model.

The ratios $v_2\{4\}/v_2\{2\}$, shown in panel (c), serve as a figure of merit for the strength of the elliptic flow fluctuations; $v_2\{4\}/v_2\{2\} = r$ correspond to minimal flow fluctuations for $r \sim 1.0$ and sizable flow fluctuations for decreasing values of $r < 1$. The computed ratios, which are similar to the experimental constructed ones, are to within $\sim 5\%$ insensitive to the model choice and the parameter sets tabulated in Tab. 1, suggesting that the flow fluctuations are eccentricity-driven and are roughly a constant fraction of $v_2\{2\}$. The $\langle p_T \rangle$ values shown in panel (d) further indicate minor sensitivity to the models and the associated model parameters.

Figure 2 compare the centrality dependence of the values for $\text{Var}(v_2^2)$ (a), $\sqrt{c_k}/\langle p_T \rangle$ (b), $\text{cov}(v_2^2, [p_T])$ (c) and $\rho(v_2^2, [p_T])$ (d), computed for tracks with $0.2 < p_T < 2.0$ GeV/c in Au+Au collisions simulated with the AMPT and EPOS models. The hatched bands represent $\text{Var}(v_2^2)$ (a) and $\sqrt{c_k}/\langle p_T \rangle$ (b) values evaluated from the experimental data reported by the STAR collaboration [63, 65]. They show good qualita-

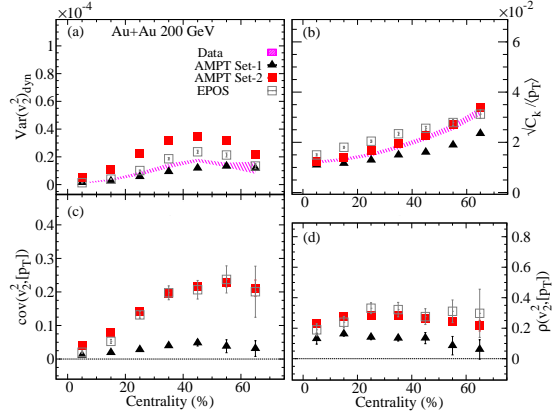


Figure 2: Comparison of the centrality dependence of $\text{Var}(v_n^2)_{\text{dyn}}$ (a), $\sqrt{c_k}/\langle p_T \rangle$ (b), $\text{cov}(v_n^2, [p_T])$ (c) and $\rho(v_n^2, [p_T])$ (d) obtained from the AMPT and EPOS models for Au+Au collisions at 200 GeV. The hatched bands represent the experimental data reported by the STAR collaboration in Refs [63, 65].

tive agreement with the theoretical values for $\text{Var}(v_2^2)$, and $\sqrt{c_k}/\langle p_T \rangle$. The comparisons show good overall agreement between the results for EPOS and those for AMPT with parameter Set-2. By contrast, panels (a) - (d) indicate sizable differences between the AMPT results for parameter Set-1 [string melting off] and Set-2 [string melting on]. These differences suggest that data-model comparisons of $\text{Var}(v_n^2)_{\text{dyn}}$, $\sqrt{c_k}/\langle p_T \rangle$, $\text{cov}(v_n^2, [p_T])$ and $\rho(v_n^2, [p_T])$ could serve as an important constraint for charting the respective roles of the partonic and hadronic phases in these collisions.

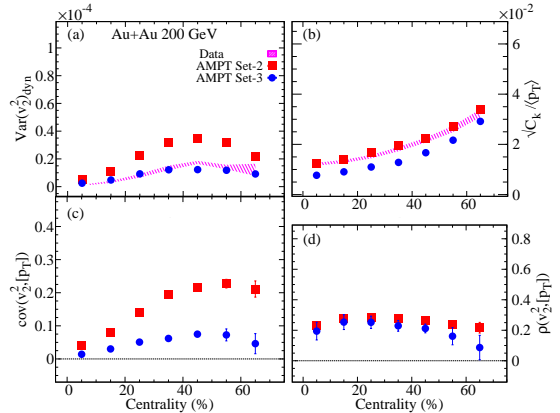


Figure 3: Comparison of the centrality dependence of the values for $\text{Var}(v_n^2)_{\text{dyn}}$ (a), $\sqrt{c_k}/\langle p_T \rangle$ (b), $\text{cov}(v_n^2, [p_T])$ (c) and $\rho(v_n^2, [p_T])$ (d), computed for Au+Au collisions at 200 GeV with the AMPT model. Results are compared for model parameter Set-2 ($\eta/s = 0.1$) and Set-3 ($\eta/s = 0.3$) as indicated. The hatched bands represent the experimental data reported by the STAR collaboration in Refs [63, 65].

Figure 3 shows the influence of η/s on the values

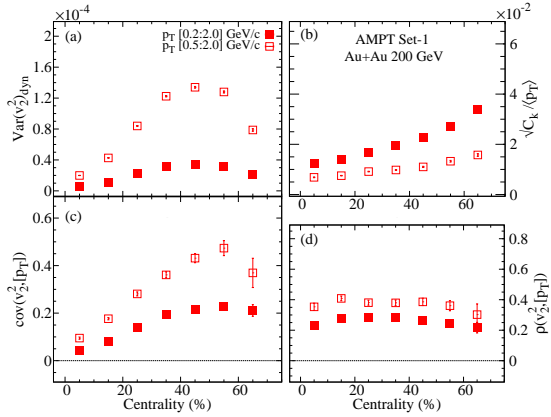


Figure 4: Comparison of the centrality-dependent values for $\text{Var}(v_2^2)_{\text{dyn}}$ (a), $\sqrt{c_k}/\langle p_T \rangle$ (b), $\text{cov}(v_2^2, [p_T])$ (c) and $\rho(v_2^2, [p_T])$ (d) computed for the selections $0.2 < p_T < 2.0 \text{ GeV}/c$ and $0.5 < p_T < 2.0 \text{ GeV}/c$ for Au+Au collisions at 200 GeV with the AMPT model .

for $\text{Var}(v_2^2)$ (a), $\sqrt{c_k}/\langle p_T \rangle$ (b), $\text{cov}(v_2^2, [p_T])$ (c) and $\rho(v_2^2, [p_T])$ (d). Here, results from the AMPT model are shown for model parameter Set-2 ($\eta/s = 0.1$) and Set-3 ($\eta/s = 0.3$) as indicated. The hatched bands represent the values for $\text{Var}(v_2^2)$ (a) and $\sqrt{c_k}/\langle p_T \rangle$ (b) constructed from the experimental data reported by the STAR collaboration [63, 65]. Figs. 3 (a) - (c) show that an increase in the magnitude of η/s reduces the values for $\text{Var}(v_2^2)$, $\sqrt{c_k}/\langle p_T \rangle$, and $\text{cov}(v_2^2, [p_T])$ for all centrality selections. By contrast, the $\rho(v_2^2, [p_T])$ values show little, if any, change, suggesting that an apparent cancellation of the effects of viscous attenuation renders the $\rho(v_2^2, [p_T])$ correlator insensitive to η/s .

Differential flow measurements $v_n(p_T)$ indicate that v_n is strongly correlated with p_T . Consequently, it is instructive to investigate the influence of a p_T cut on the $\rho(v_2^2, [p_T])$ correlator. Fig. 4 compare the extracted values for $\text{Var}(v_2^2)_{\text{dyn}}$ (a), c_k (b), $\text{cov}(v_2^2, [p_T])$ (c) and $\rho(v_2^2, [p_T])$ (d) computed for the selections $0.2 < p_T < 2.0 \text{ GeV}/c$ and $0.5 < p_T < 2.0 \text{ GeV}/c$ in Au+Au collisions ($\sqrt{s_{NN}} = 200 \text{ GeV}$) with the AMPT model. Figs. 4 (a), (c) and (d) indicate a sizable increase in the centrality-dependent values for $\text{Var}(v_2^2)_{\text{dyn}}$, $\text{cov}(v_2^2, [p_T])$ and $\rho(v_2^2, [p_T])$ with $\langle p_T \rangle$ [33]. Contrastingly, the centrality-dependent values for c_k indicate a decrease with $\langle p_T \rangle$.

The sensitivity of the $\rho(v_n^2, [p_T])$ correlator to the shape and size of the collision system was investigated using the Event Shape Engineering (ESE) technique [66]. This technique leverages the observation that selections on the magnitude of the event-by-event fluctuations of the v_n coefficients, for a fixed centrality, serve to influence the shape of the collision system [67].

The event-shape selections were performed via a frac-

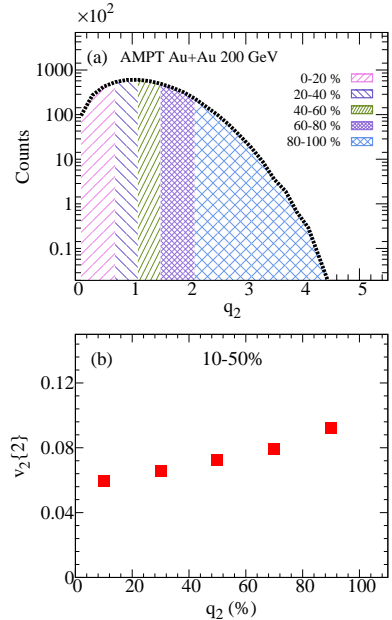


Figure 5: The q_2 distribution (a) for 10 - 50% central Au+Au collisions at $\sqrt{s_{NN}} = 200 \text{ GeV}$, obtained with the sub-event cut $1.5 < \eta < 2.5$ with the AMPT model; $v_2\{2\}$ vs. $q_2(\%)$ (b) for the q_2 selections indicated in panel (a).

tional cut on the distribution of the magnitude of the reduced second-order flow vector, q_2 , [66, 68];

$$Q_{2,x} = \sum_i \cos(2\varphi_i), Q_{2,y} = \sum_i \sin(2\varphi_i), \quad (14)$$

$$q_2 = \frac{|Q_2|}{\sqrt{M}}, |Q_2| = \sqrt{Q_{2,x}^2 + Q_{2,y}^2} \quad (15)$$

where Q_2 is the magnitude of the second-order harmonic flow vector calculated within the sub-event $1.5 < \eta < 2.5$, and M is the charged hadron multiplicity for this sub-event. The sub-event $|\eta| < 1.0$ was used to evaluate $\rho(v_n^2, [p_T])$ to ensure the separation between the sub-event used to evaluate q_2 and $\rho(v_n^2, [p_T])$. Note that there are two caveats to the ESE method. First, the q_2 selective power depends on the magnitude of v_2 and the event multiplicity, so the benefit of the technique is handicapped by weak flow values and small event multiplicities [69]. Second, the non-flow effects, such as resonance decays, jets, etc. [70], could bias the q_2 selections. The latter can be minimized via a $\Delta\eta$ separation between the sub-events used for the q_2 selections and $\rho(v_n^2, [p_T])$ evaluations. Fig. 5 (a) shows a representative q_2 distribution for 10-50% central Au+Au collisions at 200 GeV. The $v_2\{2\}$ values which result from the $q_2\%$ selections indicated in panel (a), are shown in Fig. 5 (b). They indicate an essentially linear increase of $v_2\{2\}$ with $q_2\%$.

Figure 6 compare the $q_2\%$ dependence of the values for $\text{Var}(v_2^2)$ (a), $\sqrt{c_k}/\langle p_T \rangle$ (b), $\text{cov}(v_2^2, [p_T])$ (c)

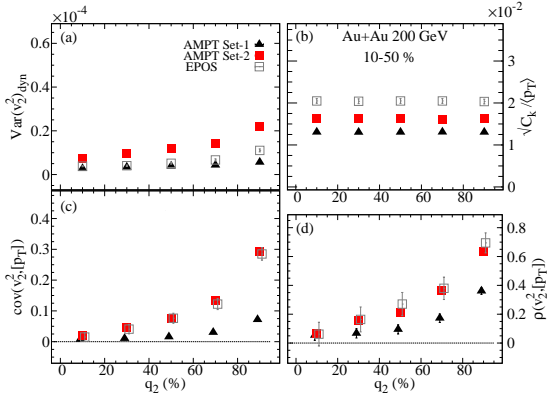


Figure 6: Comparison of the q_2 -dependent of $\text{Var}(v_n^2)_{\text{dyn}}$ (a), $\sqrt{c_k}/\langle p_T \rangle$ (b), $\text{cov}(v_n^2, [p_T])$ (c) and $\rho(v_n^2, [p_T])$ (d) computed for 10 – 50% central Au+Au collisions ($\sqrt{s_{NN}} = 200$ GeV) obtained with the AMPT and EPOS models.

and $\rho(v_n^2, [p_T])$ (d), computed for tracks with $0.2 < p_T < 2.0$ GeV/c in Au+Au collisions simulated with the AMPT and EPOS models. A striking feature of these results is the $q_2\%$ -independence of c_k and the essentially quadratic dependence of $\text{cov}(v_n^2, [p_T])$ and $\rho(v_n^2, [p_T])$ on $q_2\%$. These dependencies suggests that data-model comparisons of the $\rho(v_n^2, [p_T])$ correlators extracted in shape-engineered events, could serve as a sensitive constraint for the initial-state eccentricity, and give important insight on the deformation of colliding systems.

In summary, we have presented extensive model studies to evaluate the model dependence, as well as the response and sensitivity of the $\rho(v_n^2, [p_T])$ correlator to collision-system size and shape and the η/s of the matter produced in the collisions. We find that $\rho(v_n^2, [p_T])$ is sensitive to the event shape selections of the collision system, but insensitive to sizable changes in the η/s of the medium produced in the collisions. Initial comparisons of the calculated and experimental $\text{Var}(v_n^2)$, and $\sqrt{c_k}/\langle p_T \rangle$ values, also indicate good qualitative agreement. These findings strongly suggest that precise differential measurements of $\rho(v_n^2, [p_T])$ as a function of system-size, shape, deformation and beam-energy could provide more stringent constraints to discern between initial-state models and hence, more reliable extractions of η/s .

Acknowledgments

The authors thank Marysia Stefaniak, Emily Racow, Benjamin Schweid, and Giuliano Giacalone for useful discussions. This research is supported by the US Department of Energy, Office of Nuclear Physics (DOE NP), under contracts DE-FG02-94ER40865 (NM) and DE-FG02-87ER40331.A008 (RL).

References

- [1] E. V. Shuryak, Quark-Gluon Plasma and Hadronic Production of Leptons, Photons and Psions, Sov. J. Nucl. Phys. 28 (1978) 408. doi:10.1016/0370-2693(78)90370-2.
- [2] E. V. Shuryak, Quantum Chromodynamics and the Theory of Superdense Matter, Phys. Rept. 61 (1980) 71–158. doi:10.1016/0370-1573(80)90105-2.
- [3] B. Muller, J. Schukraft, B. Wyslouch, First Results from Pb+Pb collisions at the LHC, Ann. Rev. Nucl. Part. Sci. 62 (2012) 361–386. arXiv:1202.3233, doi:10.1146/annurev-nucl-102711-094910.
- [4] P. Danielewicz, R. A. Lacey, P. Gossiaux, C. Pinkenburg, P. Chung, J. Alexander, R. McGrath, Disappearance of elliptic flow: a new probe for the nuclear equation of state, Phys. Rev. Lett. 81 (1998) 2438–2441. arXiv:nucl-th/9803047, doi:10.1103/PhysRevLett.81.2438.
- [5] K. Ackermann, et al., Elliptic flow in Au + Au collisions at $(S(NN))^{**}(1/2) = 130$ GeV, Phys. Rev. Lett. 86 (2001) 402–407. arXiv:nucl-ex/0009011, doi:10.1103/PhysRevLett.86.402.
- [6] K. Adcox, et al., Flow measurements via two particle azimuthal correlations in Au+Au collisions at $\sqrt{s_{NN}} = 130$ -GeV, Phys. Rev. Lett. 89 (2002) 212301. arXiv:nucl-ex/0204005, doi:10.1103/PhysRevLett.89.212301.
- [7] U. W. Heinz, P. F. Kolb, Early thermalization at RHIC, Nucl. Phys. A702 (2002) 269–280. arXiv:hep-ph/0111075, doi:10.1016/S0375-9474(02)00714-5.
- [8] P. Huovinen, P. F. Kolb, U. W. Heinz, P. V. Ruuskanen, S. A. Voloshin, Radial and elliptic flow at rhic: Further predictions, Phys. Lett. B503 (2001) 58–64.
- [9] T. Hirano, K. Tsuda, Collective flow and two pion correlations from a relativistic hydrodynamic model with early chemical freeze out, Phys. Rev. C66 (2002) 054905. arXiv:nucl-th/0205043, doi:10.1103/PhysRevC.66.054905.
- [10] E. Shuryak, Why does the quark gluon plasma at RHIC behave as a nearly ideal fluid?, Prog. Part. Nucl. Phys. 53 (2004) 273–303. arXiv:hep-ph/0312227, doi:10.1016/j.ppnp.2004.02.025.
- [11] T. Hirano, U. W. Heinz, D. Kharzeev, R. Lacey, Y. Nara, Hadronic dissipative effects on elliptic flow in ultrarelativistic heavy-ion collisions, Phys.Lett. B636 (2006) 299–304. arXiv:nucl-th/0511046, doi:10.1016/j.physletb.2006.03.060.
- [12] P. Romatschke, U. Romatschke, Viscosity Information from Relativistic Nuclear Collisions: How Perfect is the Fluid Observed at RHIC?, Phys.Rev.Lett. 99 (2007) 172301. arXiv:0706.1522, doi:10.1103/PhysRevLett.99.172301.
- [13] M. Luzum, P. Romatschke, Conformal Relativistic Viscous Hydrodynamics: Applications to RHIC results at $s(NN)^{**}(1/2) = 200$ -GeV, Phys.Rev. C78 (2008) 034915. arXiv:0804.4015, doi:10.1103/PhysRevC.78.034915, 10.1103/PhysRevC.79.039903.
- [14] P. Bozek, Bulk and shear viscosities of matter created in relativistic heavy-ion collisions, Phys. Rev. C 81 (2010) 034909. arXiv:0911.2397, doi:10.1103/PhysRevC.81.034909.
- [15] H. Song, S. A. Bass, U. Heinz, T. Hirano, C. Shen, 200 A GeV Au+Au collisions serve

- a nearly perfect quark-gluon liquid, Phys. Rev. Lett. 106 (2011) 192301, [Erratum: Phys. Rev. Lett.109,139904(2012)]. [arXiv:1011.2783](#), doi:[10.1103/PhysRevLett.106.192301](#),[10.1103/PhysRevLett.109d489904](#).
- [16] J. Qian, U. W. Heinz, J. Liu, Mode-coupling effects in anisotropic flow in heavy-ion collisions, Phys. Rev. C93 (6) (2016) 064901. [arXiv:1602.02813](#), doi:[10.1103/PhysRevC.93.064901](#).
- [17] B. Schenke, S. Jeon, C. Gale, Anisotropic flow in $\sqrt{s} = 2.76$ TeV Pb+Pb collisions at the LHC, Phys.Lett. B702 (2011) 59–63. [arXiv:1102.0575](#), doi:[10.1016/j.physletb.2011.06.065](#).
- [18] D. Teaney, L. Yan, Non linearities in the harmonic spectrum of heavy ion collisions with ideal and viscous hydrodynamics, Phys. Rev. C86 (2012) 044908. [arXiv:1206.1905](#), doi:[10.1103/PhysRevC.86.044908](#).
- [19] F. G. Gardim, F. Grassi, M. Luzum, J.-Y. Ollitrault, Anisotropic flow in event-by-event ideal hydrodynamic simulations of $\sqrt{s_{NN}} = 200$ GeV Au+Au collisions, Phys.Rev.Lett. 109 (2012) 202302. [arXiv:1203.2882](#), doi:[10.1103/PhysRevLett.109.202302](#).
- [20] R. A. Lacey, D. Reynolds, A. Taranenko, N. N. Ajitanand, J. M. Alexander, F.-H. Liu, Y. Gu, A. Mwai, Acoustic scaling of anisotropic flow in shape-engineered events: implications for extraction of the specific shear viscosity of the quark gluon plasma, J. Phys. G43 (10) (2016) 10LT01. [arXiv:1311.1728](#), doi:[10.1088/0954-3899/43/10/10LT01](#).
- [21] N. Magdy, X. Sun, Z. Ye, O. Evdokimov, R. Lacey, Investigation of the Elliptic Flow Fluctuations of the Identified Particles Using the a Multi-Phase Transport Model, Universe 6 (9) (2020) 146. [arXiv:2009.02734](#), doi:[10.3390/universe6090146](#).
- [22] P. Bozek, Transverse-momentum-flow correlations in relativistic heavy-ion collisions, Phys. Rev. C 93 (4) (2016) 044908. [arXiv:1601.04513](#), doi:[10.1103/PhysRevC.93.044908](#).
- [23] G. Giacalone, J. Noronha-Hostler, J.-Y. Ollitrault, Relative flow fluctuations as a probe of initial state fluctuations, Phys. Rev. C 95 (5) (2017) 054910. [arXiv:1702.01730](#), doi:[10.1103/PhysRevC.95.054910](#).
- [24] G. Giacalone, B. Schenke, C. Shen, Observable signatures of initial state momentum anisotropies in nuclear collisions, Phys. Rev. Lett. 125 (19) (2020) 192301. [arXiv:2006.15721](#), doi:[10.1103/PhysRevLett.125.192301](#).
- [25] P. Bozek, H. Mehrabpour, Correlation coefficient between harmonic flow and transverse momentum in heavy-ion collisions, Phys. Rev. C 101 (6) (2020) 064902. [arXiv:2002.08832](#), doi:[10.1103/PhysRevC.101.064902](#).
- [26] B. Schenke, C. Shen, D. Teaney, Transverse momentum fluctuations and their correlation with elliptic flow in nuclear collision, Phys. Rev. C 102 (3) (2020) 034905. [arXiv:2004.00690](#), doi:[10.1103/PhysRevC.102.034905](#).
- [27] G. Giacalone, F. G. Gardim, J. Noronha-Hostler, J.-Y. Ollitrault, Correlation between mean transverse momentum and anisotropic flow in heavy-ion collisions, Phys. Rev. C 103 (2) (2021) 024909. [arXiv:2004.01765](#), doi:[10.1103/PhysRevC.103.024909](#).
- [28] S. H. Lim, J. L. Nagle, Exploring Origins for Correlations between Flow Harmonics and Transverse Momentum in Small Collision Systems (Unambiguous Ambiguity)[arXiv:2103.01348](#).
- [29] Measurement of flow and transverse momentum correlations in Pb+Pb collisions at $\sqrt{s_{NN}} = 5.02$ TeV and Xe+Xe collisions at $\sqrt{s_{NN}} = 5.44$ TeV with the ATLAS detector, Phys. Rev. Lett. 109d489904.
- [30] P. Bozek, W. Broniowski, Transverse-momentum fluctuations in relativistic heavy-ion collisions from event-by-event viscous hydrodynamics, Phys. Rev. C 85 (2012) 044910. [arXiv:1203.1810](#), doi:[10.1103/PhysRevC.85.044910](#).
- [31] G. Giacalone, Observing the deformation of nuclei with relativistic nuclear collisions, Phys. Rev. Lett. 124 (20) (2020) 202301. [arXiv:1910.04673](#), doi:[10.1103/PhysRevLett.124.202301](#).
- [32] G. Giacalone, Constraining the quadrupole deformation of atomic nuclei with relativistic nuclear collisions, Phys. Rev. C 102 (2) (2020) 024901. [arXiv:2004.14463](#), doi:[10.1103/PhysRevC.102.024901](#).
- [33] G. Aad, et al., Measurement of flow harmonics correlations with mean transverse momentum in lead-lead and proton-lead collisions at $\sqrt{s_{NN}} = 5.02$ TeV with the ATLAS detector, Eur. Phys. J. C 79 (12) (2019) 985. [arXiv:1907.05176](#), doi:[10.1140/epjc/s10052-019-7489-6](#).
- [34] P. Božek, R. Samanta, Higher order cumulants of transverse momentum and harmonic flow in relativistic heavy ion collisions, Phys. Rev. C 104 (1) (2021) 014905. [arXiv:2103.15338](#), doi:[10.1103/PhysRevC.104.014905](#).
- [35] Z.-W. Lin, C. M. Ko, B.-A. Li, B. Zhang, S. Pal, A Multi-phase transport model for relativistic heavy ion collisions, Phys. Rev. C72 (2005) 064901. [arXiv:nucl-th/0411110](#), doi:[10.1103/PhysRevC.72.064901](#).
- [36] H. J. Drescher, M. Hladik, S. Ostapchenko, T. Pierog, K. Werner, Parton based Gribov-Regge theory, Phys. Rept. 350 (2001) 93–289. [arXiv:hep-ph/0007198](#), doi:[10.1016/S0370-1573\(00\)00122-8](#).
- [37] K. Werner, I. Karpenko, T. Pierog, M. Bleicher, K. Mikhailov, Event-by-Event Simulation of the Three-Dimensional Hydrodynamic Evolution from Flux Tube Initial Conditions in Ultrarelativistic Heavy Ion Collisions, Phys. Rev. C 82 (2010) 044904. [arXiv:1004.0805](#), doi:[10.1103/PhysRevC.82.044904](#).
- [38] K. Werner, B. Guiot, I. Karpenko, T. Pierog, Analysing radial flow features in p-Pb and p-p collisions at several TeV by studying identified particle production in EPOS3, Phys. Rev. C 89 (6) (2014) 064903. [arXiv:1312.1233](#), doi:[10.1103/PhysRevC.89.064903](#).
- [39] G.-L. Ma, Z.-W. Lin, Predictions for $\sqrt{s_{NN}} = 5.02$ TeV Pb+Pb Collisions from a Multi-Phase Transport Model, Phys. Rev. C93 (5) (2016) 054911. [arXiv:1601.08160](#), doi:[10.1103/PhysRevC.93.054911](#).
- [40] M. R. Haque, M. Nasim, B. Mohanty, Systematic investigation of azimuthal anisotropy in Au+Au and U+U collisions at $\sqrt{s_{NN}} = 200$ GeV, J. Phys. G 46 (8) (2019) 085104. doi:[10.1088/1361-6471/ab2ba4](#).
- [41] P. P. Bhaduri, S. Chattopadhyay, Differential elliptic flow of identified hadrons and constituent quark number scaling at FAIR, Phys. Rev. C 81 (2010) 034906. [arXiv:1002.4100](#), doi:[10.1103/PhysRevC.81.034906](#).
- [42] M. Nasim, L. Kumar, P. K. Netrakanti, B. Mohanty, Energy dependence of elliptic flow from heavy-ion collision models, Phys. Rev. C 82 (2010) 054908. [arXiv:1010.5196](#), doi:[10.1103/PhysRevC.82.054908](#).
- [43] J. Xu, C. M. Ko, The effect of triangular flow

- on di-hadron azimuthal correlations in relativistic heavy ion collisions, Phys. Rev. C 83 (2011) 021903. [arXiv:1011.3750](#), doi:10.1103/PhysRevC.83.021903.
- [44] N. Magdy, O. Evdokimov, R. A. Lacey, A method to test the coupling strength of the linear and nonlinear contributions to higher-order flow harmonics via Event Shape Engineering, J. Phys. G 48 (2) (2020) 025101. [arXiv:2002.04583](#), doi:10.1088/1361-6471/abcb59.
- [45] Y. Guo, S. Shi, S. Feng, J. Liao, Magnetic Field Induced Polarization Difference between Hyperons and Anti-hyperons, Phys. Lett. B 798 (2019) 134929. [arXiv:1905.12613](#), doi:10.1016/j.physletb.2019.134929.
- [46] N. Magdy, S. Basu, V. Gonzalez, A. Marin, O. Evdokimov, R. A. Lacey, C. Pruneau, Azimuthal dependence of two-particle transverse momentum current correlations [arXiv:2105.07912](#).
- [47] N. Magdy, R. A. Lacey, Model investigation of the longitudinal broadening of the transverse momentum two-particle correlator, Phys. Rev. C 104 (1) (2021) 014907. [arXiv:2101.01555](#), doi:10.1103/PhysRevC.104.014907.
- [48] B. Zhang, ZPC 1.0.1: A Parton cascade for ultrarelativistic heavy ion collisions, Comput. Phys. Commun. 109 (1998) 193–206. [arXiv:nucl-th/9709009](#), doi:10.1016/S0010-4655(98)00010-1.
- [49] X.-N. Wang, M. Gyulassy, HIJING: A Monte Carlo model for multiple jet production in p p, p A and A A collisions, Phys. Rev. D44 (1991) 3501–3516. doi:10.1103/PhysRevD.44.3501.
- [50] M. Gyulassy, X.-N. Wang, HIJING 1.0: A Monte Carlo program for parton and particle production in high-energy hadronic and nuclear collisions, Comput. Phys. Commun. 83 (1994) 307. [arXiv:nucl-th/9502021](#), doi:10.1016/0010-4655(94)90057-4.
- [51] B.-A. Li, C. M. Ko, Formation of superdense hadronic matter in high-energy heavy ion collisions, Phys. Rev. C 52 (1995) 2037–2063. [arXiv:nucl-th/9505016](#), doi:10.1103/PhysRevC.52.2037.
- [52] J. Xu, C. M. Ko, Pb-Pb collisions at $\sqrt{s_{NN}} = 2.76$ TeV in a multiphase transport model, Phys. Rev. C 83 (2011) 034904. [arXiv:1101.2231](#), doi:10.1103/PhysRevC.83.034904.
- [53] C. R. Allton, S. Ejiri, S. J. Hands, O. Kaczmarek, F. Karsch, E. Laermann, C. Schmidt, L. Scorzato, The QCD thermal phase transition in the presence of a small chemical potential, Phys. Rev. D 66 (2002) 074507. [arXiv:hep-lat/0204010](#), doi:10.1103/PhysRevD.66.074507.
- [54] M. Bleicher, et al., Relativistic hadron hadron collisions in the ultrarelativistic quantum molecular dynamics model, J. Phys. G 25 (1999) 1859–1896. [arXiv:hep-ph/9909407](#), doi:10.1088/0954-3899/25/9/308.
- [55] S. A. Bass, et al., Microscopic models for ultrarelativistic heavy ion collisions, Prog. Part. Nucl. Phys. 41 (1998) 255–369. [arXiv:nucl-th/9803035](#), doi:10.1016/S0146-6410(98)00058-1.
- [56] H. Petersen, J. Steinheimer, G. Burau, M. Bleicher, H. Stöcker, A Fully Integrated Transport Approach to Heavy Ion Reactions with an Intermediate Hydrodynamic Stage, Phys. Rev. C 78 (2008) 044901. [arXiv:0806.1695](#), doi:10.1103/PhysRevC.78.044901.
- [57] J. Jia, S. Mohapatra, Disentangling flow and non-flow correlations via Bayesian unfolding of the event-by-event distributions of harmonic coefficients in ultrarelativistic heavy-ion collisions, Phys. Rev. C 88 (1) (2013) 014907. [arXiv:1304.1471](#), doi:10.1103/PhysRevC.88.014907.
- [58] J. Jia, M. Zhou, A. Trzupek, Revealing long-range multiparticle collectivity in small collision systems via subevent cumulants, Phys. Rev. C96 (3) (2017) 034906. [arXiv:1701.03830](#), doi:10.1103/PhysRevC.96.034906.
- [59] P. Huo, K. Gajdošová, J. Jia, Y. Zhou, Importance of non-flow in mixed-harmonic multiparticle correlations in small collision systems, Phys. Lett. B 777 (2018) 201–206. [arXiv:1710.07567](#), doi:10.1016/j.physletb.2017.12.035.
- [60] C. Zhang, J. Jia, J. Xu, Non-flow effects in three-particle mixed-harmonic azimuthal correlations in small collision systems, Phys. Lett. B792 (2019) 138–141. [arXiv:1812.03536](#), doi:10.1016/j.physletb.2019.03.035.
- [61] B. B. Abelev, et al., Event-by-event mean p_T fluctuations in pp and Pb-Pb collisions at the LHC, Eur. Phys. J. C 74 (10) (2014) 3077. [arXiv:1407.5530](#), doi:10.1140/epjc/s10052-014-3077-y.
- [62] C. Zhang, A. Behera, S. Bhatta, J. Jia, Non-flow effects in correlation between harmonic flow and transverse momentum in nuclear collisions [arXiv:2102.05200](#).
- [63] J. Adams, et al., Azimuthal anisotropy in Au+Au collisions at $s(\text{NN})^{**}(1/2) = 200\text{-GeV}$, Phys. Rev. C 72 (2005) 014904. [arXiv:nucl-ex/0409033](#), doi:10.1103/PhysRevC.72.014904.
- [64] J. Adams, et al., Transverse momentum and collision energy dependence of high $p(T)$ hadron suppression in Au+Au collisions at ultrarelativistic energies, Phys. Rev. Lett. 91 (2003) 172302. [arXiv:nucl-ex/0305015](#), doi:10.1103/PhysRevLett.91.172302.
- [65] J. Adam, et al., Collision-energy dependence of p_T correlations in Au + Au collisions at energies available at the BNL Relativistic Heavy Ion Collider, Phys. Rev. C 99 (4) (2019) 044918. [arXiv:1901.00837](#), doi:10.1103/PhysRevC.99.044918.
- [66] C. Adler, et al., Elliptic flow from two and four particle correlations in Au+Au collisions at $\sqrt{s_{NN}} = 130\text{-GeV}$, Phys. Rev. C66 (2002) 034904. [arXiv:nucl-ex/0206001](#), doi:10.1103/PhysRevC.66.034904.
- [67] B. Abelev, et al., Anisotropic flow of charged hadrons, pions and (anti-)protons measured at high transverse momentum in Pb-Pb collisions at $\sqrt{s_{NN}}=2.76$ TeV, Phys. Lett. B 719 (2013) 18–28. [arXiv:1205.5761](#), doi:10.1016/j.physletb.2012.12.066.
- [68] J. Schukraft, A. Timmins, S. A. Voloshin, Ultrarelativistic nuclear collisions: event shape engineering, Phys. Lett. B 719 (2013) 394–398. [arXiv:1208.4563](#), doi:10.1016/j.physletb.2013.01.045.
- [69] A. Bzdak, S. Esumi, V. Koch, J. Liao, M. Stephanov, N. Xu, Mapping the Phases of Quantum Chromodynamics with Beam Energy Scan [arXiv:1906.00936](#).
- [70] S. A. Voloshin, A. M. Poskanzer, R. Snellings, Collective phenomena in non-central nuclear collisions [arXiv:0809.2949](#).